Adaptive Channel Estimation Using Pilot-Embedded Data-Bearing Approach for MIMO-OFDM Systems

Chaiyod Pirak, *Member, IEEE*, Z. Jane Wang, *Member, IEEE*, K. J. Ray Liu, *Fellow, IEEE*, and Somchai Jitapunkul, *Member, IEEE*

Abstract—Multiple-input multiple-output (MIMO) orthogonal-frequency-division-multiplexing (OFDM) systems employing coherent receivers crucially require channel state information (CSI). Since the multipath delay profile of channels is arbitrary in the MIMO-OFDM systems, an effective channel estimator is needed. In this paper, we first develop a pilot-embedded data-bearing (PEDB) approach for joint channel estimation and data detection, in which PEDB least-square (LS) channel estimator and maximum-likelihood (ML) data detection are employed. Then, we propose an LS fast Fourier transform (FFT)-based channel estimator by employing the concept of FFT-based channel estimation to improve the PEDB-LS one via choosing a certain number of significant taps for constructing a channel frequency response. The effects of model mismatch error inherent in the proposed LS FFT-based estimator when considering noninteger multipath delay profiles and its performance analysis are investigated. The relationship between the mean-squared error (MSE) and the number of chosen significant taps is revealed, and hence, the optimal criterion for obtaining the optimum number of significant taps is explored. Under the framework of pilot embedding, we further propose an adaptive LS FFT-based channel estimator employing the optimum number of significant taps to compensate the model mismatch error as well as minimize the corresponding noise effect. Simulation results reveal that the adaptive LS FFT-based estimator is superior to the LS FFT-based and PEDB-LS estimators under quasi-static channels or low Doppler's shift regimes.

Index Terms—Adaptive channel estimation, least-square fast Fourier transform (LS FFT) based, multiple-input multiple-output orthogonal-frequency-division mulitplexing (MIMO-OFDM), pilot embedding, space-frequency.

I. INTRODUCTION

HIGH-SPEED data transmission services have been highly demanded in future wireless communications [1]. One promising transmission scheme to satisfy this growing demand is the orthogonal-frequency-division-multiplexing (OFDM) technique [2]. Nowadays, the OFDM communication scheme has been employed in various high-speed wireless transmission standards such as broadband wireless LAN (IEEE 802.11a) [3], digital audio broadcasting (DAB) [4], and digital video broadcasting (DVB-T) [5]. Recently, multiple-input multiple-output (MIMO)-OFDM systems have been proposed for increasing communication capacity as well as reliability of the wireless communication systems by exploiting both the spatial and frequency diversities [2], [6]. Further, the space-frequency (SF) coding for MIMO-OFDM systems have been developed for achieving such diversities in order to enhance the reception performance for high data-rate wireless communications. However, those aforementioned schemes normally need to assume accurate channel state information (CSI) for coherently decoding the transmitted data, e.g., a maximum-likelihood (ML) decoder. Therefore, channel estimation is of critical importance for MIMO-OFDM systems.

Typically a pilot or training signal, a known signal transmitted from the transmitter to the receiver, is highly desirable to obtain an accurate channel estimate. In [7], the optimal criteria of designing the training sequence in MIMO-OFDM systems were proposed. There are two main types of pilot-aided channel estimation techniques for MIMO systems: the pilot symbol assisted modulation (PSAM) technique [8], and the pilot-embedding technique [9]. Recently, we proposed a pilot-embedded data-bearing (PEDB) approach for joint channel estimation and data detection by exploiting the null-space property and the orthogonality property of the data bearer and pilot matrices [10], [11].

Various channel estimation schemes have been recently proposed for MIMO-OFDM systems [7], [12]–[19]. In [12], a linear minimum mean-squared error (LMMSE) channel estimator was proposed, in which a singular-value decomposition (SVD) is used to simplify the ordinary LMMSE channel estimator. Despite the highly accurate channel estimate of this scheme, it requires intensive computational complexity and the knowledge of the underlying channel correlation. In [13], the FFT-based channel estimation using a certain number of significant taps for estimating the channel impulse response in a temporal domain was proposed. Despite the efficient computational complexity of this scheme, it could suffer from an error floor caused by a noninteger multipath delay spread, relative to the system sampling period, in the wireless channels, known as a *model mismatch error*. The enhancement and simplification of [13] were proposed in [14] and [15], respectively. In [16], an iterative algorithm for least-square (LS) channel estimation was proposed for improving the performance of the LS channel estimation. De-

spite its efficient computation and good performance for channels with the integer multipath delay profiles, it could suffer from the model mismatch error for the channels with the noninteger multipath delay profiles. In [17], an alternative channel estimation approach using time-of-arrivals (TOA) estimation was proposed. Despite its good performance in resisting the model mismatch error, it imposes high computation complexity.

The model mismatch error or, in the other words, the leakage effect was first mentioned in single-input single-output (SISO)-OFDM systems employing the FFT-based channel estimation [20]–[22]. Without the knowledge of channel correlation information and the delay of multipath signals, there are two ways to reduce the leakage effect: 1) by changing the exponential basis functions to the polynomial basis functions in the FFT-based channel estimation [23]–[25] for SISO systems and [26] for MIMO systems and 2) by employing a proper number of significant taps to construct a channel frequency response in the FFT-based channel estimation [13]. In the former approach, the thorough investigation of the polynomial-based channel estimation for the MIMO systems has been conducted in [26]. Although this approach provides better performance than the FFT-based approach [22] under the noninteger multipath delay profiles, its performance is worse under the integer multipath delay profiles. Furthermore, this approach imposes higher computational complexity than that of the FFT-based approach, and a general rule of designing the optimum window length as well as the optimum order of the polynomial is not fully discovered. Given the efficient implementation and reliability constraints, the FFT-based approach is still attractive. However, the optimal guideline about how to choose the number of significant taps remains unsolved. Our challenge now is to find the optimal criteria for obtaining the optimum number of significant taps given that the knowledge of channel correlation information, the delay of the multipath signals, and Doppler's shift are unavailable.

The goal of this paper is to develop an efficient channel estimation scheme when employing pilot-embedding idea in MIMO-OFDM systems. The main contributions of this paper are as follows.

- Generalizing the concepts in [10] and [11], we present a PEDB approach for joint channel estimation and data detection for MIMO-OFDM systems, in which PEDB LS channel estimation and ML data detection are employed, respectively. We further propose the LS FFT-based channel estimator via choosing a certain number of significant taps for constructing a channel frequency response.
- We analyze the performance of the LS FFT-based channel estimation. Then, we reveal the relationship between the mean-squared error (MSE) and the number of chosen taps, which in turn, the optimal criterion for obtaining the optimum number of significant taps is explored.
- We study the model mismatch error of the LS FFT-based channel estimator and solve this problem by proposing an adaptive LS FFT-based channel estimation approach that employs the optimum number of taps such that the average total energy of the channels dissipating in each tap is completely captured in order to compensate the model mismatch error and minimize the noise effect.

The organization of this paper is as follows. In Section II, we briefly introduce the wireless channel and system models used in this paper. In Section III, we present the PEDB approach for joint channel estimation and data detection, including the PEDB-LS channel estimation and PEDB-ML data detection. Under this pilot-embedding framework, in Section IV, we propose the LS FFT-based channel estimator and study the performance analysis for the PEDB-LS and LS FFT-based channel estimation approaches. In Section V, we propose the adaptive LS FFT-based channel estimation for improving the performance of the LS FFT-based channel estimation. In Section VI, the performance of the proposed schemes are examined via simulations, and the conclusion is given in Section VII. For ease of later use, let $(\cdot)^T$ stands for the transpose of a matrix, $(\cdot)^H$ stands for the complex-conjugate transpose of a matrix, $\mathbf{I}$ stands for an identity matrix, and $\mathbf{0}$ stands for an all-zero-element matrix.

II. WIRELESS CHANNEL AND SYSTEM MODELS

In this section, we describe the wireless channel and system models used in this paper. A K–tone SF-coded OFDM system with L_r receive and L_t transmit antennas is considered.

The complex baseband impulse response of the wireless channel between the ath ($a = 1, \ldots, L_r$) receive antenna and the bth ($b = 1, \ldots, L_t$) transmit antenna can be described by [13]

$$h_{ab}(t, \tau) = \sum_l \gamma_l^{ab}(t) \delta(\tau - D_l^{ab}) \tag{1}$$

where D_l^{ab} is the delay of the lth path and $\gamma_l^{ab}(t)$ represents the corresponding complex amplitude. $\gamma_l^{ab}(t)$'s are modelled as wide-sense stationary (WSS), narrowband complex Gaussian processes, which are independent for different paths, and $\mathrm{E}[|\gamma_l^{ab}(t)|^2] = \sigma_l^{2ab}$ with σ_l^{2ab} being the average power of the lth path. Throughout this paper, we assume that all the signals transmitted from different transmit antennas and received at different receive antennas undergo independent fading, and the channel average power is normalized to have $\sum_l \sigma_l^{2ab} = 1$. Since we particularly consider the case where all channels have the same multipath delay profiles, we drop the superscript ab in the above parameters throughout this paper. For OFDM systems with tolerable leakage, the normalized frequency response of the OFDM systems at the kth ($k = 0, \ldots, K - 1$) subcarrier between the ath receiver and the bth transmitter can be described by [13]

$$H_{ab}(m, n, k) = \sum_{l=0}^{L-1} h_{ab}(m, n, l) F_K^{k\tau_l} \tag{2}$$

where $h_{ab}(m, n, l) \triangleq h_{ab}(m, nT_f, \tau_l t_s)$; $F_K = \exp(-j2\pi/K)$; $t_s = 1/(K\Delta f)$, with Δf being the tone spacing, is the sample interval of the system; T_f is the OFDM block length; and m denotes the index of a group of N-OFDM blocks described next. L is the number of nonzero paths, which represents the order of frequency diversity of the channel, and τ_l ($l = 0, \ldots, L - 1$) is the lth path's delay sampled at rate t_s, e.g., $D_l = \tau_l t_s$. Furthermore, the average power of $h_{ab}(m, n, l)$ and the value of $L(\leq K)$ depend on the delay profile and the dispersion of the wireless channels. For simplicity, we omit

the time index n in all notations in the next text. For OFDM systems with tolerable leakage, the delays τ_l's can be assumed as integers and L is the number of significant taps in [13]. In this paper, we consider the general case of noninteger τ_l's and deal with the corresponding leakage problem.

At the transmitter side, the data stream is split into L_t substreams, and, in each substream, a group of data is chosen to match the corresponding baseband M-phase-shift-keyed (MPSK) constellation symbol. These MPSK-data symbols are then coded by the SF block code, e.g., [6], and grouped to construct the $L_t \times KN$ SF-coded data matrix $\mathbf{S}(m)$, where N denotes the number of OFDM blocks (each OFDM block has K tones) to be regarded as one SF-coded data block, and m denotes the N-OFDM-block index. Before modulating this SF-coded data block by the OFDM modulator, the SF-coded data matrix $\mathbf{S}(m)$ is embedded by the pilot signal using the PEDB approach proposed later, so we have the SF-coded symbol matrix with size $L_t \times KM$, where M denotes the number of OFDM blocks included in one SF-coded symbol block. Notice that $M > N$ since redundancy is introduced after embedding the pilot signal for acquiring the CSI. Each pilot-embedded OFDM block is then modulated and simultaneously transmitted across L_t transmit antennas. In order to eliminate the intersymbol interference (ISI), we employ a cyclic prefix in which the length of cyclic extension must be no smaller than τ_{L-1}. In this paper, we consider two types of fading channels: quasi-static and non-quasi-static frequency-selective Rayleigh-fading channels. The former is the scenario that the channel remains constant over the SF-coded symbol block but changes in a block-by-block basis, whereas in the latter the channel changes within the SF-coded symbol block. At the receiver side, the received signal is sampled at rate t_s and demodulated by the OFDM demodulator. By assuming tolerable power leakage and perfect time/frequency synchronization, the received signal of the mth SF-coded symbol block can be described by

$$\mathbf{Y}(m) = \mathbf{H}(m)\mathbf{U}(m) + \mathbf{Z}(m) \qquad (3)$$

where $\mathbf{Y}(m)$ is a $L_r \times KM$ matrix; $\mathbf{H}(m)$ is the $L_r \times KL_t$ channel matrix in which the ath row of $\mathbf{H}(m)$ is $[\mathbf{H}_{a1}(m), \ldots, \mathbf{H}_{aL_t}(m)]$, where $\mathbf{H}_{ab}(m) = [H_{ab}(m,0), \ldots, H_{ab}(m, K-1)]$; $\mathbf{Z}(m)$ is the $L_r \times KM$ additive white Gaussian noise (AWGN) matrix with zero-mean and variance $(\sigma^2/2)\mathbf{I}_{(L_r KM \times L_r KM)}$ per real dimension; and $\mathbf{U}(m)$ is the $KL_t \times KM$-equivalent SF-coded symbol matrix. Throughout this paper, we assume that the channels and noise, and channels from different paths are mutually uncorrelated.

III. PILOT-EMBEDDED DATA-BEARING APPROACH

In this section, we first present the main ideas of the PEDB approach for joint channel estimation and data detection. We then briefly introduce the basic LS channel estimation and the ML data detection.

A. Pilot-Embedded Data-Bearing Approach

In the PEDB approach for joint channel estimation and data detection, the equivalent SF-coded symbol matrix $\mathbf{U}(m)$ can be described as follows:

$$\mathbf{U}(m) = \mathbf{D}(m)\mathbf{B} + \mathbf{C} \qquad (4)$$

where $\mathbf{D}(m)$ denotes the $KL_t \times KN$ equivalent SF-coded data matrix constructed from the matrix $\mathbf{S}(m)$ using the $K \times K$ matrix-diagonalized operator $\text{diag}\{\cdot\}$, where the $((b-1)K+1)^{\text{th}}$ row to the $(bK)^{\text{th}}$ row of $\mathbf{D}(m)$ are $[\text{diag}\{[\mathbf{S}(m)]_{b,1:K}\}, \ldots, \text{diag}\{[\mathbf{S}(m)]_{b,(N-1)K+1:NK}\}]$ with $x : y$ denotes the column/row index interval ranging from x to y; $\mathbf{B}$ is the $KN \times KM$ data bearer matrix; and $\mathbf{C}$ is the $KL_t \times KM$ pilot matrix. Notice that the K diagonal elements of a $(b,c)^{\text{th}}$ submatrix, $c = 1, \ldots, M$, represented in $\mathbf{U}(m)$ by the $((b-1)K+1)^{\text{th}}$ row to the $(bK)^{\text{th}}$ row and the $((c-1)K+1)^{\text{th}}$ column to the $(cK)^{\text{th}}$ column are the cth transmitted SF-coded OFDM block at the bth transmitter in the mth SF-coded symbol block group. In addition, the energy constraint $\mathrm{E}[\|\mathbf{D}(m)\|^2] = KL_t$ is maintained for the equivalent SF-coded data matrix. Substituting (4) into (3), we have the received signal matrix as

$$\mathbf{Y}(m) = \mathbf{H}(m)(\mathbf{D}(m)\mathbf{B} + \mathbf{C}) + \mathbf{Z}(m). \qquad (5)$$

Now, by the PEDB approach, we require that the data bearer matrix $\mathbf{B}$ and the pilot matrix $\mathbf{C}$ satisfy the following properties:

$$\mathbf{BC}^T = \mathbf{0}_{(KN \times KL_t)}, \ \mathbf{CC}^T = \alpha\mathbf{I}_{(KL_t \times KL_t)}, \qquad (6)$$

$$\mathbf{CB}^T = \mathbf{0}_{(KL_t \times KN)}, \text{ and } \mathbf{BB}^T = \beta\mathbf{I}_{(KN \times KN)} \qquad (7)$$

where β is the real-valued data-power factor and α is the real-valued pilot-power factor. The similar property $\mathbf{CC}^T = \alpha\mathbf{I}$ in (6) is also suggested in [7] that it is the optimal criterion for the optimal training design for MIMO-OFDM systems. There are at least two possible structures of data-bearing and pilot matrices, in which the elements of these matrices are real numbers, that satisfy the properties (6) and (7) as follows.

1) Time-Multiplexing-Based Matrices: The structures of time-multiplexing (TM)-based matrices are given as

$$\mathbf{B} = \sqrt{\beta}\left[\mathbf{0}_{(KN \times KL_t)}; \mathbf{I}_{(KN \times KN)}\right], M = N + L_t$$
$$\mathbf{C} = \sqrt{\alpha}\left[\mathbf{I}_{(KL_t \times KL_t)}; \mathbf{0}_{(KL_t \times KN)}\right] \qquad (8)$$

where ; stands for matrix combining. This structure has been widely used in many literatures [7] and [12]–[17].

2) Code-Multiplexing (CM)-Based Matrices: The structures of code-multiplexing (CM)-based matrices are given as

$$\mathbf{B} = \sqrt{\beta}\text{WH}[1:N]_{(N \times M)} \otimes \mathbf{I}_{(K \times K)}, M = N + L_t$$
$$\mathbf{C} = \sqrt{\alpha}\text{WH}[N+1:M]_{(L_t \times M)} \otimes \mathbf{I}_{(K \times K)} \qquad (9)$$

where $\text{WH}[x:y]$ denotes a submatrix created by splitting the $M \times M$ normalized Walsh–Hadamard matrix [27] starting from the xth row to the yth row, and $\otimes$ denotes the Kronecker

product. This structure provides an instructive example of the proposed general idea in (4) for pilot embedding.

Notice that, in (8) and (9), the proposed scheme is a block-training scheme in which L_t OFDM blocks are used for estimating the CSI. As suggested in [12] and [13], when using only one OFDM block for training in the MIMO-OFDM systems, the LS channel estimator for $\mathbf{H}_{ab}(m)$ exists only if $K \geq L_t L$. In general, in the case that $K < L_t L$ and $L \leq K$, the use of L_t OFDM blocks for training can guarantee the existence of the LS channel estimator and other better channel estimators, such as the LMMSE channel estimator [12].

B. PEDB LS Channel Estimation

We first extract the pilot part from the received signal matrix $\mathbf{Y}(m)$. By using the null-space and orthogonality properties in (6), respectively, we are able to extract the pilot part by simply postmultiplying $\mathbf{Y}(m)$ in (5) by $\mathbf{C}^T$ and then dividing by α to arrive at

$$\frac{\mathbf{Y}(m)\mathbf{C}^T}{\alpha} = \mathbf{H}(m) + \frac{\mathbf{Z}(m)\mathbf{C}^T}{\alpha}. \qquad (10)$$

Let $\mathbf{Y}_1(m) = \mathbf{Y}(m)\mathbf{C}^T/\alpha$ and $\mathbf{Z}_1(m) = \mathbf{Z}(m)\mathbf{C}^T/\alpha$, we have $\mathbf{Y}_1(m) = \mathbf{H}(m) + \mathbf{Z}_1(m)$. The PEDB-LS channel estimator can be obtained by applying the LS channel estimation approach for $\mathbf{Y}_1(m)$ to arrive at

$$\hat{\mathbf{H}}_{LS}(m) = \mathbf{Y}_1(m) = \frac{\mathbf{Y}(m)\mathbf{C}^T}{\alpha}. \qquad (11)$$

The PEDB-LS channel estimate in (11) completely captures the whole channel frequency response contaminated by AWGN. Note that it is not benefitted by using all the PEDB-LS channel estimate taps in decoding the SF-coded transmitted signal since some taps are dominated by noise, where the noise power is significantly larger than the channel energy contained. We improve the performance of PEDB-LS channel estimation by taking into consideration such fact in the Section IV.

C. PEDB ML Data Detection

We now explore the procedure of PEDB-ML data detection. First, we extract the data part from the received signal matrix $\mathbf{Y}(m)$. Using the null-space and orthogonality properties in (7), respectively, we are able to extract the data part by simply postmultiplying $\mathbf{Y}(m)$ in (5) by $\mathbf{B}^T$, and then dividing by β

$$\frac{\mathbf{Y}(m)\mathbf{B}^T}{\beta} = \mathbf{H}(m)\mathbf{D}(m) + \frac{\mathbf{Z}(m)\mathbf{B}^T}{\beta}. \qquad (12)$$

Letting $\mathbf{Y}_2(m) = \mathbf{Y}(m)\mathbf{B}^T/\beta$ and $\mathbf{Z}_2(m) = \mathbf{Z}(m)\mathbf{B}^T/\beta$, we have $\mathbf{Y}_2(m) = \mathbf{H}(m)\mathbf{D}(m) + \mathbf{Z}_2(m)$. From the orthogonality of $\mathbf{B}$ in (7), we note that $\sum_{j'=1}^{KM} |B_{i',j'}|^2 = \beta$, $\forall i'$. Therefore, the data-bearer-projected noise $\mathbf{Z}_2(m)$ is AWGN with zero-mean and variance $(\sigma^2/2\beta)\mathbf{I}_{(KL_rN \times KL_rN)}$ per real dimension. Due to the i.i.d white Gaussian distribution of $\mathbf{Z}_2(m)$, the PEDB-ML receiver jointly decides the codewords

for the dth OFDM block in the mth SF-coded data block by solving the following minimization problem:

$$\hat{\mathbf{D}}_{i,j}(m) = \min_{\mathbf{D}_{i,j}} \|\mathbf{Y}_{2_{s,j}}(m) - \hat{\mathbf{H}}_{s,i}(m)\mathbf{D}_{i,j}(m)\|^2$$

$$i = 1 : KL_t, \; j = (d-1)K+1 : dK$$

$$s = 1 : L_r, \; \text{and} \; d = 1, \dots, N \qquad (13)$$

where $\hat{\mathbf{H}}(m)$ is the estimated channel matrix, e.g., $\hat{\mathbf{H}}(m) = \hat{\mathbf{H}}_{LS}(m)$. The codeword transmitted from the bth transmitter is represented by $\hat{\mathbf{D}}_{i_b,j}(m)$, with $i_b = (b-1)K+1 : bK$.

IV. LS FFT-BASED CHANNEL ESTIMATION AND PERFORMANCE ANALYSIS

As mentioned earlier, the PEDB-LS channel estimate contains the channel frequency response that is contaminated by AWGN. By properly choosing the significant taps and discarding the rest less significant taps, we can reconstruct the whole channel frequency response in which the excessive noise contained in the less significant taps are completely cancelled. In this section, we improve the performance of the PEDB-LS estimator in (11) by employing the basic concepts of the FFT-based approach in [13]. First, following the description in Section III, we propose the LS FFT-based channel estimator and point out an inherent problem. Then, we analyze their channel estimation performances.

A. LS FFT-Based Channel Estimation Approach

As suggested in [13], the FFT-based channel estimation approach first calculates the temporal LS channel estimate by using L significant taps. The resulting temporal LS channel estimate is then FFT transformed to obtain the K-subcarrier channel frequency response. The simplified approach was also suggested in [13] by choosing P significant taps (i.e., P's largest $\sum_{b=1}^{L_t} |\hat{H}_{LS_{ab}}(m,k)|^2$ are selected) instead of using L significant taps.

Now let us describe the LS FFT-based channel estimator under the proposed framework in details. From (11), we have $\hat{\mathbf{H}}_{LS_{ab}}(m) = ([\hat{\mathbf{H}}_{LS}(m)]_{a,(b-1)K+1:bK})^T$. From the channel model in (2), $\hat{\mathbf{H}}_{LS_{ab}}(m)$ can be expressed as

$$\hat{\mathbf{H}}_{LS_{ab}}(m) = \mathbf{F}\mathbf{h}_{ab}(m) + \mathbf{Z}_{1_{ab}}(m) \qquad (14)$$

where $\mathbf{F}$ is the $K \times L$ matrix whose element $[\mathbf{F}]_{xy}$ is defined by $\exp[(-j2\pi/K)(x-1)\tau_y]$, $x = 1, \dots, K$, $y = 0, \dots, L-1$; $\mathbf{h}_{ab}(m) = [h_{ab}(m,0), \dots, h_{ab}(m,L-1)]^T$; and $\mathbf{Z}_{1_{ab}}(m) = ([\mathbf{Z}_1(m)]_{a,(b-1)K+1:bK})^T$. Notice that the LS estimate in (14) indeed represents the K-tap LS FFT-based estimate for a^{th} receive and b^{th} transmit antennas.

Transforming the PEDB-LS estimator in (14) to the temporal one by using the $K \times K$ IFFT matrix $\mathbf{G}$, whose element $[\mathbf{G}]_{xy}$ is defined by $(1/K)\exp(j2\pi/K)(x-1)(y-1), x, y = 1, \dots, K$, we have

$$\hat{\mathbf{h}}_{LS_{ab}}(m) = \mathbf{G}\hat{\mathbf{H}}_{LS_{ab}}(m) = \mathbf{G}\mathbf{F}\mathbf{h}_{ab}(m) + \mathbf{G}\mathbf{Z}_{1_{ab}}(m). \qquad (15)$$

From the fact that $[\mathbf{GF}]_{xy} = (f(x - 1 - \tau_y)/K)\exp(j\xi(x - 1 - \tau_y))$, $x = 1,\ldots,K$, $y = 0,\ldots,L - 1$, where $f(q) = \sin(\pi q)/\sin(\pi q/K)$ is the leakage function and $\xi = (K - 1)\pi/K$, substituting this fact into (15) results in

$$\mathbf{GFh}_{ab}(m) = \frac{1}{K}\left[\sum_{l=0}^{L-1} h_{ab}(m,l)f(-\tau_l)e^{j\xi(-\tau_l)},\ldots,\right.$$

$$\left.\sum_{l=0}^{L-1} h_{ab}(m,l)f(K - 1 - \tau_l)e^{j\xi(K-1-\tau_l)}\right]^T . \quad (16)$$

Note that if q is equal to an integer number, then $f(q) = 0$; if q is equal to zero, then $f(0) = K$. Let $\mathbf{Z}_{1_{ab}}^G(m) = \mathbf{GZ}_{1_{ab}}(m)$, then substituting $\mathbf{Z}_{1_{ab}}^G(m)$ and (16) into (15), we have

$$\hat{\mathbf{h}}_{LS_{ab}}(m) = [g(1),\ldots,g(K)]^T \quad (17)$$

where

$$g(x) = \frac{1}{K}\sum_{l=0}^{L-1} h_{ab}(m,l)f(x - 1 - \tau_l)e^{j\xi(x-1-\tau_l)} + Z_{1_{ab}}^G(m,x)$$

with $Z_{1_{ab}}^G(m,x)$ being the xth element of $\mathbf{Z}_{1_{ab}}^G(m)$.

Obviously, from $g(x)$, if τ_l is an integer, then the lth element of the L largest elements of $\hat{\mathbf{h}}_{LS_{ab}}(m)$ is equal to $h_{ab}(m,l) + Z_{1_{ab}}^G(m,l)$, and the remaining elements are equal to $Z_{1_{ab}}^G(m,e)$, $e \neq l$, $e \in \{0,\ldots,K - 1\}\backslash\mathcal{W}_1$ with $\mathcal{W}_1$ being the set of the L largest elements. As a result, choosing L largest taps and replacing the $(K - L)$ remaining taps by zero is sufficient and optimal, resulting in the LS FFT-based estimate of the temporal channel impulse response $\hat{\mathbf{h}}_{\text{FFT}_{ab}}(m)$, since we completely capture the channel impulse response $\mathbf{h}_{ab}(m)$, and remove the excessive noise in the $(K-L)$ remaining taps. However, in reality, the lth multipath delay τ_l is often noninteger; hence, the L-multipath channel impulse response dissipates to all K taps of $\hat{\mathbf{h}}_{LS_{ab}}(m)$ and thus results in the *model mismatch error*, which increases the channel estimation error, primarily caused by the AWGN $\mathbf{Z}_{1_{ab}}^G(m)$. This model mismatch error causes the severe error floor in the MSE and the detection error probability. Once the L or P largest taps are chosen and the rest taps are replaced by zero, the LS FFT-based estimated channel frequency response is given as

$$\hat{\mathbf{H}}_{\text{FFT}_{a,b}}(m) = K\mathbf{G}^H\hat{\mathbf{h}}_{\text{FFT}_{ab}}(m). \quad (18)$$

It is worth mentioning that, for our problem, we do not assume any knowledge of channel correlation information, Doppler's shift, or the delay of the multipath signals, so we simply use $\hat{\mathbf{h}}_{\text{FFT}_{ab}}(m)$ for constructing the whole channel frequency response in (18). In addition, if the additional information about channel correlation or Doppler's shift are available, the robust channel estimator proposed in [22] can be adopted to enhance the performance of the LS FFT-based channel estimation.

B. Channel Estimation Error Performance Analysis

We now analyze the performance of the PEDB-LS and LS FFT-based channel estimators by using the MSE of channel estimation as the performance measure.

1) PEDB-LS Channel Estimator: For arbitrary multipath delay profiles, the temporal channel impulse response between the ath receiver and b^{th} transmitter can be described by, as in (16), $\mathbf{h}_{ab}^G(m) = \mathbf{GFh}_{ab}(m)$.

The channel estimation error can be readily described by

$$\tilde{\mathbf{h}}_{LS_{ab}}(m) = \mathbf{h}_{ab}^G(m) - \hat{\mathbf{h}}_{LS_{ab}} = -\mathbf{Z}_{1_{ab}}^G(m) \quad (19)$$

by referring to $\hat{\mathbf{h}}_{LS_{ab}}(m)$ in (15), and $\mathbf{h}_{ab}^G(m)$. Using (19), the $\text{MSE}_{LS}(a, b)$ of the channel estimation is expressed as

$$\text{MSE}_{LS}(a, b) = \text{E}[\|\tilde{\mathbf{h}}_{LS_{ab}}(m)\|^2] = \frac{\sigma^2}{\alpha} \quad (20)$$

by using $\text{E}[|Z_{1_{ab}}^G(m,x)|^2] = \sigma^2/K\alpha$, $x = 1,\ldots,K$, as referring to Section III-B. It is worth noticing that (20) is also the MSE of the K-tap FFT-based channel estimation.

For L_r-receiver L_t-transmitter MIMO systems, the overall MSE_{LS} in (20) can be expressed as follows:

$$\text{MSE}_{LS}^T = \sum_{a=1}^{L_t}\sum_{b=1}^{L_r}\text{MSE}_{LS}(a, b) = \frac{\sigma^2 L_t L_r}{\alpha}. \quad (21)$$

2) LS FFT-Based Channel Estimator: As we mentioned earlier, the LS FFT-based channel estimator first simply chooses the L largest taps and then replaces the $(K - L)$ remaining taps by zero. This operation can be equivalently described by using the $K \times K$ tap-selection matrix $\mathbf{T}$ given by

$$\mathbf{T} = \text{diag}\{1, 1,\ldots,0, 1,\ldots,0\}, \quad (22)$$

where 0's and 1's represent nonselected and selected taps, respectively. There are $(K - L)$ 0's and L 1's elements in the diagonal elements of $\mathbf{T}$. By using the tap-selection matrix $\mathbf{T}$, the temporal LS FFT-based estimate of the channel impulse response between the ath receiver and b^{th} transmitter can be described by

$$\hat{\mathbf{h}}_{\text{FFT}_{ab}}(m) = \mathbf{TG}\hat{\mathbf{H}}_{LS_{ab}}(m)$$
$$= \mathbf{TGFh}_{ab}(m) + \mathbf{TGZ}_{1_{ab}}(m) \quad (23)$$

by plugging in $\hat{\mathbf{H}}_{LS_{ab}}(m)$ in (14).

Similarly to (19), the channel estimation error can be described by using $\mathbf{h}_{ab}^G(m)$ and $\hat{\mathbf{h}}_{\text{FFT}_{ab}}(m)$ in (23)

$$\tilde{\mathbf{h}}_{\text{FFT}_{ab}}(m) = \mathbf{h}_{ab}^G(m) - \hat{\mathbf{h}}_{\text{FFT}_{ab}}(m)$$
$$= (\mathbf{GF} - \mathbf{TGF})\mathbf{h}_{ab}(m) - \mathbf{TGZ}_{1_{ab}}(m). \quad (24)$$

Now let us define $\mathcal{W}_2 \in \{0,\ldots,K - 1\}\backslash\mathcal{W}_1$ to be a set of the nonselected $(K - L)$ less significant taps, and $w_2 \in \mathcal{W}_2$ and

$w_1 \in \mathcal{W}_1$ are row indexes indicating the 0's and 1's elements of $\mathbf{T}$, respectively. It can be shown that

$$[\mathbf{GF} - \mathbf{TGF}]_{w_2, 1:L} = \frac{1}{K}[f(w_2 - 1)e^{j\xi(w_2 - 1)}, \ldots,$$
$$f(w_2 - 1 - \tau_{L-1})e^{j\xi(w_2 - 1 - \tau_{L-1})}] \quad (25)$$

by using $\tau_0 = 0$. Therefore, by substituting (25) into (24), we have

$$[(\mathbf{GF} - \mathbf{TGF})\mathbf{h}_{ab}(m)]_{w_1 \in \mathcal{W}_1}$$
$$= [\mathbf{TGZ}_{1_{ab}}(m)]_{w_2 \in \mathcal{W}_2} = 0$$
$$[(\mathbf{GF} - \mathbf{TGF})\mathbf{h}_{ab}(m)]_{w_2 \in \mathcal{W}_2}$$
$$= \frac{1}{K}\sum_{l=0}^{L-1} h_{ab}(m,l)f(w_2 - 1 - \tau_l)e^{j\xi(w_2 - 1 - \tau_l)} \text{ and }$$
$$[\mathbf{TGZ}_{1_{ab}}(m)]_{w_1 \in \mathcal{W}_1} = [\mathbf{Z}_{1_{ab}}^G(m)]_{w_1 \in \mathcal{W}_1}. \quad (26)$$

From (26), it is readily shown that the channel estimation error of the LS FFT-based channel estimator are due to two error sources: the model mismatch error, i.e., $[(\mathbf{GF} - \mathbf{TGF})\mathbf{h}_{ab}(m)]_{w_2 \in \mathcal{W}_2}$, and the corresponding noise effect, i.e., $[\mathbf{TGZ}_{1_{ab}}(m)]_{w_1 \in \mathcal{W}_1}$. By substituting (26) into (24), we have the following $\mathrm{MSE}_{\mathrm{FFT}}(a,b)$:

$$\mathrm{MSE}_{\mathrm{FFT}}(a,b) = \mathrm{E}[\|\tilde{\mathbf{h}}_{\mathrm{FFT}_{ab}}(m)\|^2] = \epsilon + \frac{L\sigma^2}{K\alpha} \quad (27)$$

where $\epsilon = (1/K^2)\sum_{w_2 \in \mathcal{W}_2}\sum_{l=0}^{L-1}\mathrm{E}[|h_{ab}(m,l)f(w_2 - 1 - \tau_l)|^2]$, and the second equality is obtained by using the assumption that the channel and noise, and channels from different paths are mutually uncorrelated. For L_r-receiver L_t-transmitter MIMO systems, the overall $\mathrm{MSE}_{\mathrm{FFT}}$ in (27) can be expressed as follows:

$$\mathrm{MSE}_{\mathrm{FFT}}^T = \chi + \frac{L\sigma^2 L_t L_r}{K\alpha} \quad (28)$$

where

$$\chi = \frac{1}{K^2}\sum_{a=1}^{L_r}\sum_{b=1}^{L_t}\sum_{w_2 \in \mathcal{W}_2}\sum_{l=0}^{L-1}\mathrm{E}[|h_{ab}(m,l) \cdot f(w_2 - 1 - \tau_l)|^2]. \quad (29)$$

It can be shown that

$$\chi \triangleq \chi_1 - \chi_2, \quad (30)$$

where $\chi_1 = \sum_{a=1}^{L_r}\sum_{b=1}^{L_t}\sum_{j=1}^{K}\sum_{l=0}^{L-1}\mathrm{E}[|h_{ab}(m,l)f(j-1-\tau_l)|^2]$ and

$$\chi_2 = \sum_{a=1}^{L_r}\sum_{b=1}^{L_t}\sum_{w_1 \in \mathcal{W}_1}\sum_{l=0}^{L-1}\mathrm{E}[|h_{ab}(m,l) \cdot f(w_1 - 1 - \tau_l)|^2].$$

From the fact that $(1/K^2)\chi_1 + \eta_1 = \sum_{a=1}^{L_r}\sum_{b=1}^{L_t}\sum_{j=1}^{K}\mathrm{E}[\|[\hat{\mathbf{h}}_{LS_{ab}}(m)]_j\|^2] - \eta_2$, where $\eta_1 = L\sigma^2 L_t L_r/K\alpha$ and $\eta_2 = (K-L)\sigma^2 L_t L_r/K\alpha$, and that

$(1/K^2)\chi_2 + \eta_1 = \sum_{a=1}^{L_r}\sum_{b=1}^{L_t}\sum_{w_1 \in \mathcal{W}_1}\mathrm{E}[\|[\hat{\mathbf{h}}_{LS_{ab}}(m)]_{w_1}\|^2]$, we have

$$\frac{\chi}{K^2} = \sum_{a=1}^{L_r}\sum_{b=1}^{L_t}\sum_{j=1}^{K}\mathrm{E}[\|[\hat{\mathbf{h}}_{LS_{ab}}(m)]_j\|^2] - \eta_2$$
$$- \sum_{a=1}^{L_r}\sum_{b=1}^{L_t}\sum_{w_1 \in \mathcal{W}_1}\mathrm{E}[\|[\hat{\mathbf{h}}_{LS_{ab}}(m)]_{w_1}\|^2]. \quad (31)$$

First, we consider the case of the multipath delay profiles with integer delays. In this case, the model mismatch error χ is equal to zero, as explained in Section IV-A. Hence, the minimum MSE of the LS FFT-based channel estimation is given by

$$\mathrm{MSE}_{\mathrm{FFT}_{\min}}^T = \frac{L\sigma^2 L_t L_r}{K\alpha}. \quad (32)$$

It is worth noticing that, since $L \leq K$, (32) is always less than or equal to (21), meaning that the channel estimation performance of the LS FFT-based channel estimator is superior to that of the PEDB-LS channel estimator when the multipath delay profiles are with integer delays.

Using $\chi = 0$ for the case of the multipath delay profiles with integer delays, we have

$$\sum_{a=1}^{L_r}\sum_{b=1}^{L_t}\sum_{w_1 \in \mathcal{W}_1}\mathrm{E}[\|[\hat{\mathbf{h}}_{LS_{ab}}(m)]_{w_1}\|^2]$$
$$= \sum_{a=1}^{L_r}\sum_{b=1}^{L_t}\sum_{j=1}^{K}\mathrm{E}[\|[\hat{\mathbf{h}}_{LS_{ab}}(m)]_j\|^2] - \frac{(K-L)\sigma^2 L_t L_r}{K\alpha}. \quad (33)$$

Therefore, (33) can be used as the optimal criterion in choosing the set $\mathcal{W}_1$ which indicates the indexes of the L significant taps, in order to achieve the minimum MSE. This observation in (33) indicates that in order to achieve the minimum MSE of the LS FFT-based channel estimator, the L largest chosen taps must be capable of capturing the average total energy of channels in the presence of AWGN. This alternative optimal criterion, based on the average total energy criterion, is useful, especially in the implementation point of view because it indeed links directly to the minimum MSE criterion, in which the knowledge about the exact CSI is required in its unrealistic computation.

Further, we consider the case of the noninteger multipath delay profiles. In this case, the model mismatch error χ is nonzero due to the leakage, as shown in (30). It is important to study the joint effects of the tap length L and the noise level σ^2 on the MSE measure. From the definition of the model mismatch error χ, it is straightforward to see that, as the number of selected taps L increases, the error χ decreases, so does the first term in (28); however, the resulting noise effect contained in these selected taps is inevitably increased, as shown by the second term in (28). On the other hand, as decreasing L, the error χ is increased, whereas the resulting noise effect is decreased. This tradeoff between the model mismatch error and noise effect is very crucial to the MIMO system performances. In what follows, we propose an improvement of the LS FFT-based channel estimator to overcome such problems.

V. PROPOSED ADAPTIVE LS FFT-BASED CHANNEL ESTIMATOR

In this section, we propose an adaptive LS FFT-based channel estimator in which the number of taps used in channel estimation can be adjustable in order to minimize the model mismatch error and the corresponding noise effect. The model mismatch error in the LS FFT-based estimator described in Section IV stems from the fact that a fixed number of L (or P) largest taps is used in the estimation process for all signal-to-noise ratio (SNR) values. It has been suggested in [13] that, in low-SNR regimes, the channel estimation error is mainly caused by the AWGN; hence, a small number of taps is recommended to reduce the noise effect; as a result, a smaller overall channel estimation error is possible. In high-SNR regimes, the channel estimation error is mainly caused by the model mismatch error; hence, a large number of taps is suggested to compensate such mismatch error. Based on this basic idea, we propose the adaptive LS FFT-based approach, in which the number of taps P is chosen to achieve the intuitive goal that the average total energy of the channels dissipating in each tap is completely captured in order to compensate the model mismatch error. Specifically, we propose that the number of taps P_{opt} used to capture the CSI in $\hat{\mathbf{h}}_{LS_{ab}}(m)$ in (17) is obtained by solving the optimization problem in (34).

$$P_{\text{opt}}$$
$$= \min(P) \text{ s.t. } \sum_{a=1}^{L_r}\sum_{b=1}^{L_t} \mathrm{E}\left[\max_{\mathcal{W}_p, |\mathcal{W}_p|=P}\sum_{i\in\mathcal{W}_p}||[\hat{\mathbf{h}}_{LS_{ab}}(m)]_i||^2\right]$$
$$\geq \sum_{a=1}^{L_r}\sum_{b=1}^{L_t}\sum_{j=1}^{K}\mathrm{E}[||[\hat{\mathbf{h}}_{LS_{ab}}(m)]_j||^2] - \frac{(K-P)L_tL_r\sigma^2}{K\alpha}. \quad (34)$$

It is clear that, for a given P, the solution of achieving $\max_{\mathcal{W}_p, |\mathcal{W}_p|=P}\sum_{i\in\mathcal{W}_p}||[\hat{\mathbf{h}}_{LS_{ab}}(m)]_i||^2$ is to choose $\mathcal{W}_p$ as the indexes of the P largest taps.

Now let us intuitively explain why (34) in details. If we assume a perfect situation, then the most desired criteria used to determine the number of significant taps P is the MSE in (28) such that the optimization solution is given as

$$P_{\text{opt}} = \min_{P}\{\text{MSE}_{\text{FFT}}^T(P)\}. \quad (35)$$

First, instead of minimizing $\text{MSE}_{\text{FFT}}^T(P)$ directly, we want to take advantage of specific observations revealed in the two terms of (28). In (31), we can see that choosing $L = K$ yields a zero model mismatch error χ. To illustrate the effects of P (i.e., $P = L$ in (28) and (31)) and σ^2 on the overall MSE measure, considering a specific scenario as in Section VI, in Fig. 1, we plot the corresponding χ/K^2 term and the noise error term $L\sigma^2L_tL_r/K\alpha$ as a function of P under several SNR levels. From this figure, we note that χ/K^2 converges to zero as P increases, meaning that more taps can be used to compensate the model mismatch error. In addition, it is seen that the resulting P_{opt} increases as SNR increases. In addition, it is noted that P_{opt} can be approximately determined by locating the intersection point of the curve of the model mismatch error and the curve of
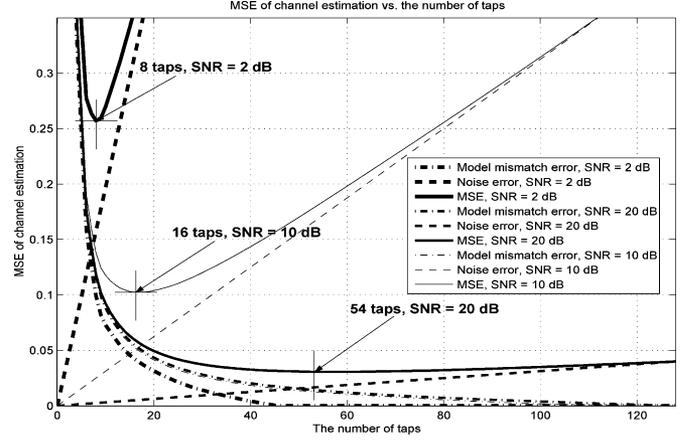
Fig. 1. Theoretical examples of the model mismatch error, the noise effect, and the overall MSE of the LS FFT-based channel estimator as a function of the number of significant taps P. Here, the perfect situation is assumed.

the noise error. Therefore, based on the above observation, the problem described in (35) can be formulated as

$$P_{\text{opt}} = \min(P) \text{ s.t. } \left\{\frac{\chi}{K^2} \leq \frac{P\sigma^2L_tL_r}{K\alpha}\right\}. \quad (36)$$

By substituting (31), the problem in (36) can be equivalently described as (37).

$$P_{\text{opt}} = \min(P) \text{ s.t.}$$
$$\sum_{a=1}^{L_r}\sum_{b=1}^{L_t}\sum_{i\in\mathcal{W}_p}\mathrm{E}\left[||[\hat{\mathbf{h}}_{LS_{ab}}(m)]_i||^2\right] + \frac{P\sigma^2L_tL_r}{K\alpha}$$
$$\geq \left(\sum_{a=1}^{L_r}\sum_{b=1}^{L_t}\sum_{j=1}^{K}\mathrm{E}[||[\hat{\mathbf{h}}_{LS_{ab}}(m)]_j||^2] - \frac{(K-P)L_tL_r\sigma^2}{K\alpha}\right). \quad (37)$$

However, in practice, since $\mathcal{W}_p$ is an unknown set, it is not feasible to compute the term

$$\sum_{a=1}^{L_r}\sum_{b=1}^{L_t}\sum_{i\in\mathcal{W}_p}\mathrm{E}\left[||[\hat{\mathbf{h}}_{LS_{ab}}(m)]_i||^2\right]$$

directly. Instead, for each transmission, depending on the real observations, for different P, we instantaneously compute the term $\max_{\{\mathcal{W}_p, |\mathcal{W}_p|=P\}}\sum_{i\in\mathcal{W}_p}||[\hat{\mathbf{h}}_{LS_{ab}}(m)]_i||^2$. Then, empirical expectation is calculated. Overall, we compute the following term:

$$\sum_{a=1}^{L_r}\sum_{b=1}^{L_t}\mathrm{E}\left[\max_{W_p, |W_p|=P}\sum_{i\in W_p}||[\hat{\mathbf{h}}_{LS_{ab}}(m)]_i||^2\right].$$

Since

$$\sum_{a=1}^{L_r}\sum_{b=1}^{L_t}\mathrm{E}\left[\max_{\mathcal{W}_p, |\mathcal{W}_p|=P}\sum_{i\in\mathcal{W}_p}||[\hat{\mathbf{h}}_{LS_{ab}}(m)]_i||^2\right]$$
$$\geq \sum_{a=1}^{L_r}\sum_{b=1}^{L_t}\sum_{i\in\mathcal{W}_p}\mathrm{E}\left[||[\hat{\mathbf{h}}_{LS_{ab}}(m)]_i||^2\right] \quad (38)$$
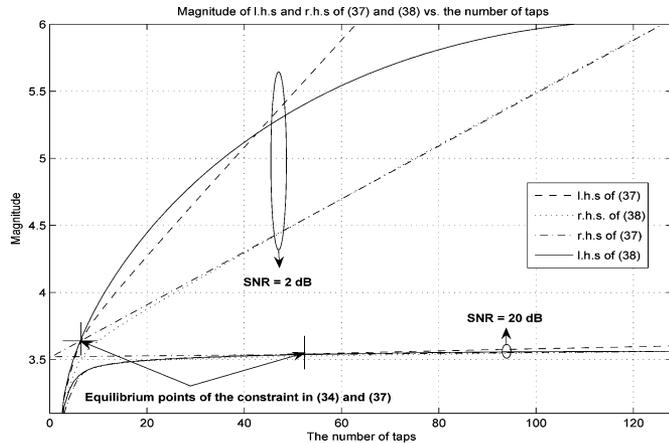
Fig. 2. Relationship between LHS and RHS of (37) and (38) based on numerical calculations.

Fig. 3. Illustration of the number of taps of the proposed scheme in (34) compared with the optimum number of taps obtained from an exhaustive search for the minimum $\mathrm{MSE}_{\mathrm{FFT}}^{T}$ in (28) in two different power delay profiles: typical urban and two-ray power delay profiles with delay spread of 5 μs.

where $\mathcal{W}_p$ is a set of the P largest taps. In low-SNR regimes, the left-hand side (LHS) of (38) is much larger than that of right-hand side (RHS) because of the large noise variance. In high-SNR regimes, the LHS of (38) is much closer to that of the RHS because of the small noise variance. Intuitively, we can see that the LHS consists of both the RHS and the noise effect. We note that the left hand is based on order statistics. In our case, since the components in $\hat{\mathbf{h}}_{LS_{ab}}(m)$ follow nonidentical distributions, due to the complex nature of order statistics, it is infeasible to find the theoretical close-form expression of the LHS of (38) in term of the RHS of (38). Due to the inequality in (38), one question we are interested in is how close the difference between the LHS and the RHS of (38) to the noise error $L\sigma^2 L_t L_r/K\alpha$ is. Numerical examples are plotted in Fig. 2 to demonstrate the relationship between the LHS of (37) and the LHS of (38). From Fig. 2, we can see that the curves of the LHS of (37) and (38) are close together when the number of taps are small until the intersection point between these two curves and the RHS of (37) for both SNR = 2 and 20 dB. This phenomenon indicates that by replacing the LHS of (37) by the LHS of (38) for determining the minimum number of taps that yield the equality to the constraint of (37), the resulting number of taps are mostly the same as solving (37) directly. It is worth noticing that in the regimes beyond the intersection point, these two curves are different; however, this phenomenon does not affect the minimum number of taps since we never exploit their relationship in these regimes.

Based on the above observations, we propose to replace the LHS of (37) by the LHS of (38), and thus replace the inequality constraint in (37) by the inequality constraint in (34). Therefore, we have the proposed scheme in determining P_{opt} as described in (34). In this sense, we could regard the proposed scheme in (34) as a suboptimal approach in determining P_{opt}. However, as illustrated in Fig. 3, in most cases, the P_{opt} determined by solving the problem in (34) is almost identical to the optimum solution obtained by using an exhaustive search for the minimum $\mathrm{MSE}_{\mathrm{FFT}}^{T}$ in (28). While the latter case is not practical, it serves as a theoretical ideal solution. Further, studying the problem described in (34), we can see that in low-SNR regimes, due to the large noise variance, a small number of taps is enough
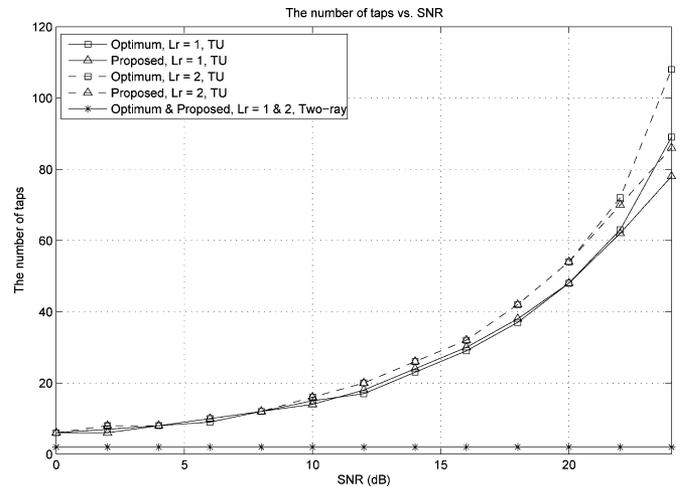
to make the constraint of (34) exist. In high-SNR regimes, a large number of taps is needed, as we expected, in order to make the constraint of (34) exist. These results are consistent with our intuitions. The equality will be held for (38) if and only if $\sigma^2 = 0$ or $P = K$. In addition, the setting parameters of the experiment in Fig. 3 are described is Section VI.

We want to emphasize that the solution of (34) is the optimum number of taps for the LS FFT-based channel estimator in the sense that the average total energy of the channels dissipating in each tap is completely captured by using the P_{opt} significant taps; as a result, the minimum model mismatch error as well as the minimum corresponding noise effect are achieved.

VI. SIMULATION RESULTS

To illustrate the performance of the proposed scheme, simulations are conducted under two scenarios: quasi-static and nonquasi-static frequency-selective Rayleigh-fading channels. The simulated SF block code uses Alamouti's structure, as proposed in [6], whose elements are taken from a binary phase-shift keying (BPSK) constellation for two transmit and two receive antennas. The COST207 typical urban (TU) six-ray normalized power delay profile [13] with a delay spread of 5 μs is studied. The entire channel bandwidth, 1 MHz, is divided into $K = 128$ subcarriers in which four subcarriers on each end are served as guard tones, and the rest (120 tones) are used to transmit data. To make the tone orthogonal to each other, the symbol duration is 128 μs, and an additional 20-μs guard interval is used as the cyclic prefix length to eliminate the ISI. This results in a total block length $T_f = 148$ μs and a subchannel symbol rate $r_b = 6.756$ KBd.

In addition, the equal block-power allocation, i.e., $\beta = \alpha = 0.5$ W, is employed, the normalized SF-coded symbol block-power is 1 W, the number of transmit antennas L_t is 2, $N = 2$, and $M = N + L_t = 4$. To illustrate the performance of the proposed adaptive LS FFT-based channel estimation versus the PEDB-LS and LS FFT-based channel estimations, both TM-
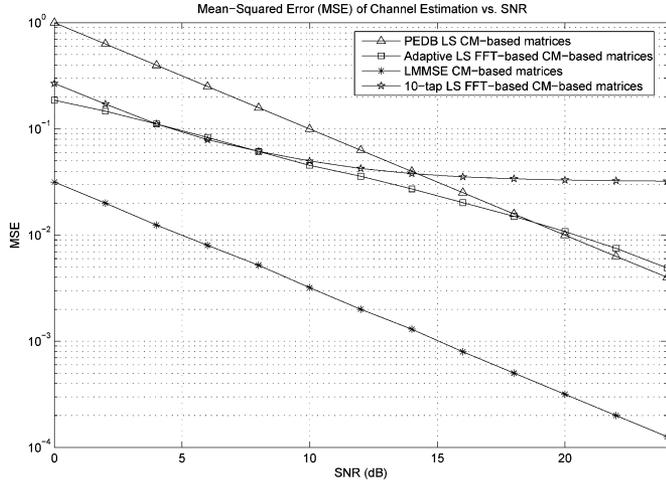
Fig. 4. The graph of MSEs of the channel estimation in quasi-static fading channels.

Fig. 5. Graph of BERs of the pilot-embedded SF-coded MIMO-OFDM system in quasi-static fading channels.

and CM-based structures in (8) and (9), respectively, are examined.

A. Quasi-Static Channel Scenario

In this scenario, the channel impulse response $h_{ab}(m,l)$'s in (2) are from the normalized time-varying channel, which is modeled as Jake's model [28], when $f_d * T_f = 0.08$ (fast fading) with f_d being the Doppler's shift. In addition, since the performances of both TM- and CM-based structures are the same in this scenario, we only show the performances of the CM-based structure.

In Fig. 4, the MSEs of the PEDB-LS, 10-tap LS FFT-based, adaptive LS FFT-based, and LMMSE channel estimators [12] are shown. Notice that the PEDB-LS estimator has a highest MSE in low-SNR regimes among all other channel estimators. This is due to the severe noise effect corrupting in all K channel estimate taps, whereas the other schemes employ small number of taps resulting in the lower noise effect. In high-SNR regimes, the PEDB-LS and adaptive LS FFT-based channel estimators performs better than the 10-tap LS FFT-based channel estimator in which the error floor caused by the model mismatch error occurs, whereas the former two do not suffer from this severe error floor since they employ more taps and thus result in a lower model mismatch error. It is worth noticing that the LMMSE channel estimator serves as the channel estimation performance bound at the price of the intensive computational complexity and the additional information about channel correlation.

In Fig. 5, the BERs of the SF-coded MIMO-OFDM system employing different channel estimators are shown. Notice that the 10-tap LS FFT-based, and adaptive LS FFT-based channel estimator performances are quite close in low-SNR regimes, whereas the PEDB-LS channel estimator performs worse, in which the 2-dB SNR difference compared to the former two channel estimators, at BER of 10^{-3}, is observed. In high-SNR regimes, the 10-tap LS FFT-based channel estimator suffers from the error floor, say at BER of 2×10^{-4}, whereas the adaptive LS FFT-based and the PEDB-LS channel estimators do not. At BER of 10^{-4}, the SNR differences between the ideal-channel scheme, where the true channel impulse response is employed,
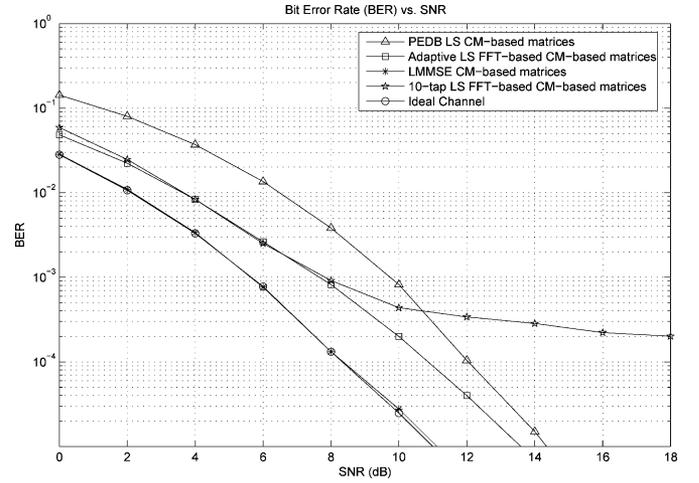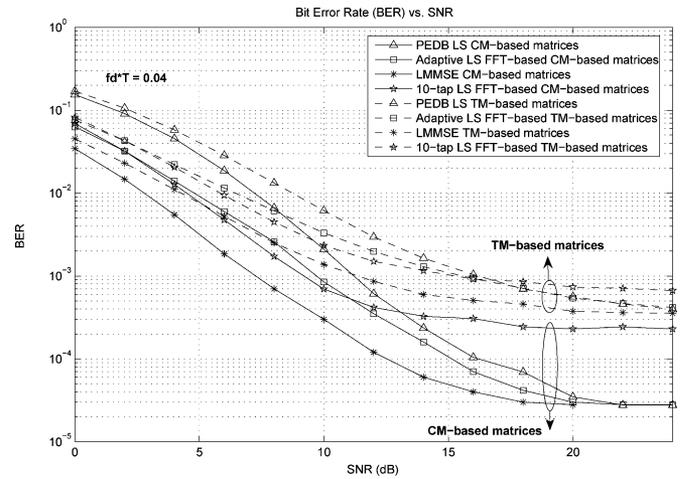
Fig. 6. Graph of BERs of the pilot-embedded SF-coded MIMO-OFDM system in non-quasi-static fading channels with $f_d * T_f = 0.04$.

and the adaptive LS FFT-based and PEDB-LS channel estimators are 2.2 dB and 3.6 dB, respectively, whereas the LMMSE channel estimator provides the error probability that coincides with the ideal-channel scheme.

B. Nonquasi-Static Channel Scenario

For the sake of exposition, we study a four-block fading model in which the channel impulse response $h_{ab}(m,l)$ symmetrically changes four times within one SF-coded symbol block, i.e., there exists $\mathbf{H}_1(m)$ to $\mathbf{H}_4(m)$ in the mth-block SF-coded symbol matrix.

In Figs. 6 and 7, the BERs of the SF-coded MIMO-OFDM system employing the PEDB-LS, 10-tap LS FFT-based, adaptive LS FFT-based, and LMMSE channel estimators, when $f_d * T_f$ are 0.04 and 0.064, are shown, respectively. Notice that, in Fig. 6, when the Doppler's shift is small ($f_d * T_f = 0.04$) in high-SNR regimes, the PEDB-LS, adaptive LS FFT-based, and LMMSE channel estimators are superior to the 10-tap LS FFT-based estimator. In low-SNR regimes, the PEDB-LS estimator performs the worst resulting from the severe noise effect. In Fig. 7, when Doppler's shift is high ($f_d * T_f = 0.064$)
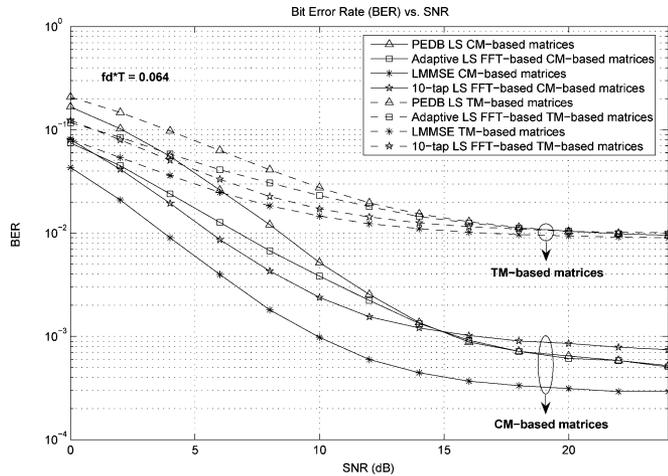
Fig. 7. Graph of BERs of the pilot-embedded SF-coded MIMO-OFDM system in non-quasi-static fading channels with $f_d * T_f = 0.064$.

in high-SNR regimes, all channel estimators yields quite close results. This phenomenon stems from the fact that the channel mismatch error dominates all factors causing the detection error. It is worth noticing the CM structure outperforms the TM structure, where the latter suffers from the highest error floor, as reported in [10] and [11].

VII. CONCLUSION

In this paper, we have presented a PEDB framework for joint channel estimation and data detection and proposed an adaptive LS FFT-based channel estimator to improve the performances of the LS FFT-based and PEDB-LS channel estimators. The optimal criterion for obtaining the optimum number of significant taps for the adaptive LS FFT-based estimator was also discovered. Simulations were conducted to examine the performance of the proposed schemes. For quasi-static TU-profile fading channels, the adaptive LS FFT-based estimator shows superior performance to that of the 10-tap LS FFT-based and PEDB-LS estimators. For instance, at BER of 10^{-4}, the SNR differences are as 2.2 dB and 3.6 dB, respectively, for the adaptive LS FFT-based and the PEDB-LS estimators compared with the ideal-channel scheme, whereas the 10-tap LS FFT-based channel estimator suffers from the severe error floor caused by the model mismatch error. For the nonquasi-static TU-profile fading channels, under low Doppler's shift regimes, the adaptive estimator is the best in high-SNR regimes; however, in the low-SNR regimes, the performance of the PEDB-LS approach is the worst and the other three estimators are comparable. Furthermore, under high Doppler's shift regimes, the channel mismatch error dominates all factors causing the detection error, and thus results in comparable error floors for all channel estimators. In addition, the LMMSE channel estimator serves as a performance bound.

REFERENCES

[1] T. Ojanperä and R. Prasad, "An overview of third generation wireless personal communications: A European perspective," *IEEE Pers. Commun.*, vol. 5, pp. 59–65, Dec. 1998.

[2] L. J. Cimini Jr. and N. R. Sollenberger, "OFDM with diversity and coding for high-bit-rate mobile data applications," in *Proc. IEEE Global Telecommunications (IEEE GLOBECOM) Conf.*, Pheonix, AZ, Nov. 1997, pp. 305–309.

[3] *Wireless LAN Medium Access Control (MAC) and Physical Layer (PHY) Specifications: High-Speed Physical Layers in the 5 GHz Band*, IEEE Std 802.11a, Sep. 1999.

[4] *Radio Broadcasting Systems; Digital Audio Braodcasting (DAB) to Mobile, Portable and Fixed Receivers*, ETS 300 401, 1997.

[5] *Digital Video Broadcasting (DVB) Framing Structure, Channel Coding and Modulation Digital Terestrail Television (DVB-T)*, ETS 300 744, v1.2.1, 1999.

[6] W. Su, Z. Safar, M. Olfat, and K. J. R. Liu, "Obtaining full-diversity space-frequency codes from space-time codes via mapping," *IEEE Trans. Signal Process.*, vol. 51, no. 11, pp. 2905–2916, Nov. 2003.

[7] I. Barhumi, G. Leus, and M. Moonen, "Optimal training design for MIMO-OFDM systems in mobile wireless channels," *IEEE Trans. Signal Process.*, vol. 51, no. 6, pp. 1615–1624, Jun. 2003.

[8] B. Hassibi and B. M. Hochwald, "How much training is needed in multiple-antenna wireless links?," *IEEE Trans. Inf. Theory*, vol. 49, pp. 951–963, Apr. 2003.

[9] H. Zhu, B. Farhang-Boroujeny, and C. Schlegel, "Pilot embedding for joint channel estimation and data detection in MIMO communication systems," *Commun. Lett.*, vol. 7, pp. 30–32, Jan. 2003.

[10] C. Pirak, Z. J. Wang, K. J. R. Liu, and S. Jitapunkul, "Performance analysis for pilot-embedded data-bearing approach in space-time coded MIMO systems," in *Proc. IEEE Int. Conf. Acoustics, Speech, Signal Processing (ICASSP)*, Philadelphia, PA, Mar. 2005, pp. 593–596.

[11] C. Pirak, Z. J. Wang, K. J. R. Liu, and S. Jitapunkul, "A data-bearing approach for pilot-aiding in space-time coded MIMO systems," presented at the IEEE 63rd Vehicular Technology Conf. (VTC), Melbourne, Australia, May 2006.

[12] Y. Gong and K. B. Lataief, "Low complexity channel estimation for space-time coded wideband OFDM systems," *IEEE Trans. Wireless Commun.*, vol. 2, no. 5, pp. 876–882, Sep. 2003.

[13] Y. Li, "Channel estimation for OFDM systems with transmitter diversity in mobile wireless channels," *IEEE J. Sel. Areas Commun.*, vol. 17, no. 3, pp. 461–471, Mar. 1999.

[14] Y. Li, J. H. Winters, and N. R. Sollenberger, "MIMO-OFDM for wireless communications: Signal detection with enhanced channel estimation," *IEEE Trans. Commun.*, vol. 50, no. 9, pp. 1471–1477, Sep. 2002.

[15] Y. Li, "Simplified channel estimation for OFDM systems with multiple transmit antennas," *IEEE Trans. Wireless Commun.*, vol. 1, no. 1, pp. 67–75, Jan. 2002.

[16] Y. Qiao, S. Yu, P. Su, and L. Zhang, "Research on an iterative algorithm of LS channel estimation in MIMO OFDM systems," *IEEE Trans. Broadcast.*, vol. 51, no. 1, pp. 149–153, Mar. 2005.

[17] Z. J. Wang, Z. Han, and K. J. R. Liu, "A MIMO OFDM channel estimation approach using time of arrivals," *IEEE Trans. Wireless Commun.*, vol. 4, no. 3, pp. 1207–1213, May 2005.

[18] C. Pirak, Z. J. Wang, K. J. R. Liu, and S. Jitapunkul, "Adaptive pilot-embedded data-bearing approach channel estimation in space-frequency coded MIMO-OFDM systems," presented at the 63rd IEEE Vehicular Technology Conf. (VTC), Melbourne, Australia, May 2006.

[19] C. Pirak, Z. J. Wang, K. J. R. Liu, and S. Jitapunkul, "LS FFT-based channel estimators using pilot-embedded data-bearing approach in space-frequency coded MIMO-OFDM systems," presented at the IEEE Wireless Communications Networking Conf. (WCNC), Las Vegas, NV, Apr. 2006.

[20] J. J. van de Beek, O. Edfors, M. Sandell, S. K. Wilson, and P. O. Borjesson, "On channel estimation in OFDM systems," in *Proc. 45th IEEE Vehicular Technology Conf. (VTC)*, Chicago, IL, Jul. 1999, pp. 815–819.

[21] O. Edfors, J. J. van de Beek, S. K. Wilson, M. Sandell, and P. O. Borjesson, "OFDM channel estimation by singular value decomposition," *IEEE Trans. Commun.*, vol. 46, no. 7, pp. 931–939, Jul. 1998.

[22] Y. Li, L. J. Cimini, and N. R. Sollenberger, "Robust channel estimation for OFDM systems with rapid dispersive fading channels," *IEEE Trans. Commun.*, vol. 46, pp. 902–915, Jul. 1998.

[23] M.-X. Chang and Y. T. Su, "Model-based channel estimation for OFDM signals in Rayleigh fading," *IEEE Trans. Commun.*, vol. 50, no. 4, pp. 540–544, Apr. 2002.

[24] X. Wang and K. J. R. Liu, "Channel estimation for multicarrier modulation systems using a time-frequency polynomial model," *IEEE Trans. Commun.*, vol. 50, no. 7, pp. 1045–1048, Jul. 2002.

[25] C. Pandana, Y. Sun, and K. J. R. Liu, "Channel-aware priority transmission scheme using joint channel estimation and data loading for OFDM systems," *IEEE Trans. Signal Process.*, vol. 53, no. 8, pp. 3297–3310, Aug. 2005.

[26] X. Wang and K. J. R. Liu, "Model based channel estimation framework for MIMO multicarrier communication systems," *IEEE Trans. Wireless Commun.*, vol. 4, no. 3, pp. 1–14, May 2005.

[27] A. V. Geramita and J. Seberry, *Orthogonal Designs*. New York: Marcel Dekker, 1979.

[28] W. C. Jakes Jr., "Multipath interference," in *Microwave Mobile Communication*, W. C. Jakes, Jr., Ed. New York: Wiley, 1974, pp. 67–68.

Chaiyod Pirak (M'05) received the B.Eng. degree (first-class honor (Hons. I)) in telecommunication engineering from King Mongkut's Institute of Technology Ladkrabang, Bangkok, Thailand, in 2000. He is currently working towards the Ph.D. degree in electrical engineering at Chulalongkorn University, Bangkok, Thailand, in association with the University of Maryland, College Park, MD.

He was appointed as a Research Assistance at the University of Maryland, College Park, under the joint research program between Chulalongkorn University and University of Maryland, College Park, from 2003 to 2005. His research interest is in digital signal processing for wireless communications, including array signal processing, beamforming, interference cancellation techniques, channel estimation for space-time-coded MIMO systems and space-frequency-coded MIMO-OFDM systems, CDMA systems, and cooperative communications.

Mr. Pirak received a Ph.D. scholarship from Commission on Higher Education, Ministry of Education, Royal Thai Government, for being a faculty member at King Mongkut's Institute of Technology North Bangkok after his graduation.

Z. Jane Wang (M'02) received the B.Sc. degree (with highest honors) from Tsinghua University, China, in 1996 and the M.Sc. and Ph.D. degrees from the University of Connecticut, Storrs, in 2000 and 2002, respectively, all in electrical engineering.

She was a Research Associate of Electrical and Computer Engineering Department and Institute for Systems Research at the University of Maryland, College Park. Since August 2004, she has been an Assistant Professor with the Department Electrical and Computer Engineering at the University of British Columbia (UBC), Canada. She co-edited a book titled *Genomic Signal Processing and Statistics* and coauthored a book titled *Multimedia Fingerprinting Forensics for Traitor*. Her research interests are in the broad areas of statistical signal processing, with applications to information security, biomedical imaging, genomic, and wireless communications.

Dr. Wang received the Outstanding Engineering Doctoral Student Award while at the University of Connecticut. She was a corecipient of the *EURASIP Journal on Applied Signal Processing* (JASP) Best Paper Award in 2004 and the *Junior Early Career Scholar Award* from the Peter Wall Institute at UBC in 2005. She is an Associate Editor for the *EURASIP Journal on Bioinformatics and Systems Biology*.

K. J. Ray Liu (F'03) received the B.S. degree from the National Taiwan University, Taiwan, R.O.C., in 1983 and the Ph.D. degree from the University of California, Los Angeles (UCLA) in 1990, both in electrical engineering.

He is Professor and Director of Communications and Signal Processing Laboratories of the Electrical and Computer Engineering Department and the Institute for Systems Research, University of Maryland, College Park. His research contributions encompass broad aspects of wireless communications and networking, information forensics and security, multimedia communications and signal processing, bioinformatics and biomedical imaging, and signal processing algorithms and architectures.

Dr. Liu is the recipient of numerous honors and awards, including Best Paper awards from the IEEE Signal Processing Society, the IEEE Vehicular Technology Society, and EURASIP; the IEEE Signal Processing Society Distinguished Lecturer; the EURASIP Meritorious Service Award; and the National Science Foundation Young Investigator Award. He also received the Poole and Kent Company Senior Faculty Teaching Award from the A. James Clark School of Engineering, and the Invention of the Year Award, both from University of Maryland. He is Vice President—Publications and on the Board of Governor of the IEEE Signal Processing Society. He was the Editor-in-Chief of the *IEEE Signal Processing Magazine* and the founding Editor-in-Chief of the *EURASIP Journal on Applied Signal Processing*.

Somchai Jitapunkul (M'90) received the B.Eng. and M.Eng. degrees in electrical engineering from Chulalongkorn University, Thailand, in 1972 and 1974, respectively, and the D.E.A. and Dr. Ing. degrees in "Signaux et Systems Spatio-Temporels" from Aix-Marseille University, Marseille, France, in 1976 and 1978, respectively.

He was appointed as a Lecturer in the Department of Electrical Engineering at Chulalongkorn University in 1972, Assistant Professor in 1980, and Associate Professor in 1983. In 1993, he was the founder of Digital Signal Processing Research Laboratory, where he became the head of this laboratory from 1993 to 1997. From 1997 to 1999 and 1999 to 2003, he was appointed as the head of Communication Division and the head of the Department, respectively. He also held the position of Associate Dean for Information Technology, Faculty of Engineering from 1993 to 1995. His current research interests are in image and video processing, speech and character recognition, signal compression, DSP in telecommunication, software-defined radio, smart antenna, and medical signal processing.